Nuclear import time and transport efficiency depend on importin β concentration

Weidong Yang and Siegfried M. Musser

Department of Molecular and Cellular Medicine, The Texas A&M University System Health Science Center, College Station, TX 77843

Although many components and reaction steps necessary for bidirectional transport across the nuclear envelope (NE) have been characterized, the mechanism and control of cargo migration through nuclear pore complexes (NPCs) remain poorly understood. Single-molecule fluorescence microscopy was used to track the movement of cargos before, during, and after their interactions with NPCs. At low importin β concentrations, about half of the signal-dependent cargos that interacted with an NPC were translocated across the NE, indicating a nuclear import efficiency of ∼50%. At high importin β concentrations, the import efficiency increased to ∼80% and the transit speed increased approximately sevenfold. The transit speed and import efficiency of a signal-independent cargo was also increased by high importin β concentrations. These results demonstrate that maximum nucleocytoplasmic transport velocities can be modulated by at least ∼10-fold by the importin β concentration and therefore suggest a potential mechanism for regulating the speed of cargo traffic across the NE.

Introduction

Nuclear pore complexes (NPCs) mediate the bidirectional transport of proteins, RNAs, and ribonucleoprotein cargos across the double-membrane nuclear envelope (NE) of eukaryotic cells. NPCs are large (∼60–120 megadaltons) structures with octagonal rotational symmetry. They are composed of at least 30 different nuclear pore proteins (Nups), each present in an integer multiple of eight copies (Rout and Aitchison, 2001; Cronshaw et al., 2002; Fahrenkrog and Aebi, 2003). As observed by electron microscopy, the pore itself is ∼90 nm in length and is ∼50 nm wide at its narrowest point. Flexible filaments extend ∼50 nm into the cytoplasm, and a filamentous open basket structure extends ∼75 nm into the nucleoplasm (Fahrenkrog and Aebi, 2003; Stoffler et al., 2003). Molecules smaller than ∼20–40 kD (diameter ∼4–5 nm) transit through the NPC without specific recognition ("passive diffusion" or "signal-independent transport"). Larger molecules up to ∼25 megadaltons (diameter ∼40 nm) typically form a complex with at least one transport receptor for transit through the NPC ("facilitated translocation" or "carrier-mediated, signal-dependent transport"); in most cases, the transport receptor belongs to the importin/exportin superfamily (Panté and Kann, 2002; Fahrenkrog and Aebi, 2003; Fried and Kutay, 2003).

Importins and exportins (also known as karyopherins) recognize nuclear localization sequences and nuclear export sequences, respectively, and migrate with cargos through NPCs (Nakielny and Dreyfuss, 1999). Import complexes (ICs), consisting of cargo and importins, are disassembled after transit through the NPC by RanGTP, the GTP-bound form of the G-protein Ran. Export complexes, consisting of cargo, exportin, and RanGTP, release cargos after transport through the action of Ran-binding proteins (RanBPs) and RanGAP, Ran's cytoplasmically localized GTPase activating protein (Coutavas et al., 1993; Bischoff et al., 1994; Yokoyama et al., 1995; Bischoff and Görlich, 1997; Izaurralde et al., 1997; Walther et al., 2002). A RanGTP concentration gradient is established and maintained by cytoplasmic RanGAP and nucleoplasmic RanGEF, the chromosome bound guanine-nucleoside exchange factor for Ran, which catalyzes GDP/GTP exchange (Izaurralde et al., 1997). This RanGTP concentration gradient across the NE is quite steep, as the nuclear RanGTP concentration typically exceeds the cytoplasmic concentration by ∼1,000-fold (Görlich et al., 2003). The direction of net cargo flux is determined by the RanGTP concentration gradient because transport directionality was reversed by gradient inversion (Nachury and Weis, 1999).

An extensive network of thousands of phenylalanine-glycine (FG) repeat motifs located on almost half the Nups (FG-Nups) provides binding sites for importins and exportins. These FG-Nups are distributed throughout the NPC structure on

Correspondence to Siegfried M. Musser: smusser@tamu.edu

both the cytoplasmic filaments and nuclear basket and within the pore itself (Bayliss et al., 1999; Stoffler et al., 1999; Rout, 2000; Rout and Aitchison, 2001; Cronshaw et al., 2002). The FG-repeat regions are natively unfolded (disordered) and highly flexible (Denning et al., 2003). Over half of the mass of the FG-repeat domains on the FG-Nups can be deleted without loss of viability or the permeability barrier (Strawn et al., 2004). The structure, distribution, and properties of the FG-Nups have been intensely debated. It is clear that these FG-Nups regulate passage through the ∼50-nm-diameter open pore visualized by structural studies (Fahrenkrog and Aebi, 2003; Stoffler et al., 2003) and that they play critical roles in selectivity and permeability regulation (Strawn et al., 2004). Members of the importin (Imp) β superfamily of transport receptors allow signal-dependent cargos to gain access to the pore and, ultimately, to migrate across the NE via interactions with the FG-Nup network (Rout, 2000; Ben-Efraim and Gerace, 2001; Macara, 2001; Ribbeck and Görlich, 2001; Fahrenkrog and Aebi, 2003; Fried and Kutay, 2003; Pyhtila and Rexach, 2003; Rout et al., 2003; Strawn et al., 2004; Peters, 2005).

Numerous distinct models have been postulated to explain the precise mechanism whereby molecules gain access to and subsequently translocate through the NPC (Rexach and Blobel, 1995; Koepp and Silver, 1996; Nachury and Weis, 1999; Rout, 2000; Ben-Efraim and Gerace, 2001; Macara, 2001; Ribbeck and Görlich, 2001; Pyhtila and Rexach, 2003; Rout et al., 2003; Peters, 2005). None of these models addresses the possible functional effects, such as changes in transport speed or import efficiency, that could result when multiple cargo complexes or transport cofactors simultaneously interact with the same NPC. Studies using cargo-decorated colloidal gold particles indicated that multiple import and export cargos can simultaneously bind to an NPC (Feldherr et al., 1984; Dworetzky and Feldherr, 1988), suggesting that multiple import and export cargos can simultaneously transit through the NPC. Consequently, considering the thousands of FG-repeat motifs providing binding sites, the many transport cofactors that must be recycled through the NPCs, and the massive amount of material that must pass through NPCs (Ribbeck and Görlich, 2001), the general picture that has emerged is one of two-way traffic in which multiple cargos, as well as multiple empty transport cofactors (Bayliss et al., 1999), all simultaneously migrate through a given NPC. This picture of multiple-cargo, simultaneous two-way traffic suggests that the identity and amount of material in transit at any one time could significantly affect transport speed or import efficiency. Here, import efficiency is defined as the number of cargos that enter the nucleus after ICs interact with an NPC divided by the total number of ICs that interact with that NPC. As a result of the RanGTP gradient, RanGTP is more readily available near the nucleoplasmic exit of the pore rather than near the cytoplasmic exit. Thus, for cargos that require RanGTP to exit from the NPC, a reasonable prediction is that IC dissociation and cargo exit occur preferentially near the nucleoplasmic exit. Such a situation would seemingly promote a relatively high import efficiency, though it could be significantly influenced by the distribution of RanGTP within or near the pore or by the traffic level within the NPC.

We showed earlier that the model cargo NLS-2xGFP interacts with NPCs for ∼9 ms at low IC concentrations. At high IC concentrations, this cargo accumulates in the nucleus at a rate of up to ∼1 translocation event per NPC per ms (Yang et al., 2004). One interpretation of these findings is that ∼9 ICs can transit simultaneously through a single NPC at high IC concentrations, consistent with the picture gleaned from the colloidal gold experiments discussed in the previous paragraph. However, this explanation implicitly assumes that the cargo translocation time is invariant with the IC concentration. Herein, we show that the translocation time of both signal-independent and -dependent cargos is not invariant and that one factor that influences the translocation time is the Imp β concentration. We report import efficiency measurements and demonstrate that the Imp β concentration also affects the import efficiency. The most parsimonious explanation is that the Imp β concentration within the NPC can directly and/or indirectly influence the transport speed and import efficiency.

Results

Single-molecule nuclear transport assay

We used single-molecule fluorescence (SMF) microscopy to determine interaction times and import efficiencies for an IC consisting of NLS-2xGFP(4C), Imp α, and Imp β. The four maleimide-reactive cysteines of NLS-2xGFP(4C) were used for dye labeling (Alexa 555 or 647). Images were obtained at 500 or 1,000 frames per second. Solution viscosity was increased through the addition of 25% glycerol to reduce the bulk diffusion rate. Under these conditions, an IC's originating and destination compartment was identified for 37% of NPC interaction events (Fig. 1 and Videos 1 and 2, available at http://www.jcb.org/cgi/content/full/jcb.200605053/DC1). For the remaining interaction events, the cargo could not be tracked before and/or after interaction with an NPC because of diffusion outside the focal plane. Unless otherwise noted, all single-molecule transport videos were collected within the 1-min time window beginning ∼1 min after initiating transport. A series of control experiments indicated that transport was minimally affected by the presence of 25% glycerol or the dyes on the cargo protein. In addition, single-molecule diffusion measurements indicated that our in vitro viscosity conditions very closely matched the in vivo viscosity (Figs. S1 and S3 and the supplemental text).

Under these conditions, in vitro single-molecule import experiments revealed that some cargos crossed the NE (entry events), whereas other cargos returned to the cytoplasmic compartment after interaction with NPCs (abortive events; Fig. 1). An overlay of trajectories for entry and abortive events suggests that the regions within the NPC accessible to cargos that passed through to the nucleus and those accessible to cargos that aborted transport were similar (Fig. 2 A). Thus, cargos appear to be able to penetrate fairly deeply into the NPC in cases of abortive transport. These data are consistent with a picture in which cargos randomly diffuse within a relatively large region of the NPC before exiting. Under the conditions of Fig. 1, the NPC interaction times for entry and abortive events were the same
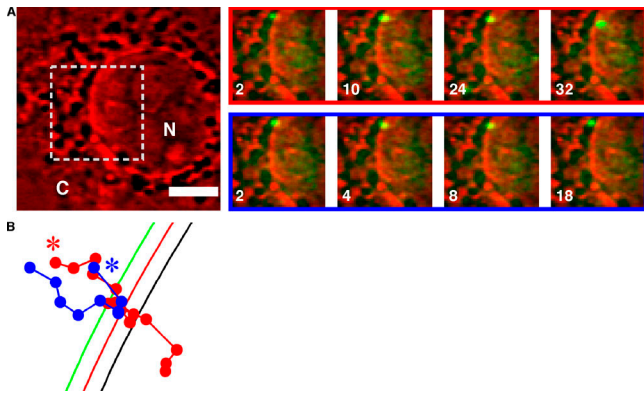
Figure 1. **Imaging of cargos before, during, and after their interaction with NPCs.** (A) Select video frames for two ICs that interacted with the same NPC in a permeabilized HeLa cell. The large image is a false-color bright-field image showing the nucleus (N) and the cytoplasm (C). The smaller images, corresponding to the boxed region in the large image (same scale), are 2-ms video frames for a cargo molecule that transported into the nucleus (top) and for a cargo molecule that underwent abortive transport, returning to the cytoplasm (bottom). These smaller images consist of SMF signals (green) overlaid onto a bright-field image (red) obtained with the same camera. The circular laser illumination area for SMF approximately filled the boxed region. The fluorescent cargo was NLS-2xGFP(4C) labeled with four Alexa 647 molecules. Numbers correspond to time in milliseconds. [fluorescent cargo] = 0.1 nM; [Imp α] = [Imp β] = 0.5 μM; [Ran] = 2 μM; [GTP] = 1 mM; [NTF2] = 1 μM. Bar, 5 μm. (B) Trajectories for the two interaction events shown in A with all frames included. The trajectory of the cargo molecule that transported into the nucleus (entry event) is shown in red, and the trajectory of the cargo molecule that underwent abortive transport (abortive event) is shown in blue. The beginning of each trajectory is identified by an asterisk. The red curve is the experimentally determined position of the NE from the bright-field image; the green and black curves are for reference at −100 and +100 nm from the NE, respectively.

($\sim$8.3 ms), within experimental error (Fig. 2, B and C), and the import efficiency was 51 ± 5%.

Interaction times and transport efficiencies change with conditions

Having established that the interaction time and import efficiency could be measured at a very low cargo concentration, we measured these parameters at higher, more physiological cargo concentrations. Because very low fluorescent cargo concentrations were essential for detection of single molecules, nonfluorescent cargo was added to the import reactions to increase the total cargo concentration. The interaction time dropped from 8.6 ± 0.4 to 2.2 ± 0.1 ms when the IC concentration was increased from 0.1 nM to 15 μM. The import efficiency increased from 51 ± 5 to 77 ± 5% over the same concentration range (Fig. 3 A).

The interaction time, import efficiency, and bulk nuclear accumulation rate indicated that an average of $\sim$1–2 ICs at a time interacted with the NPC when the IC concentration was $\sim$5 μM. Therefore, we sought an explanation as to how the interaction time could decrease approximately threefold as the IC concentration was increased from 0.1 nM to 5 μM (Fig. 3 A, red) with so few ICs within the large NPC structure. One possibility we considered was that the NPC structure exhibits hysteresis, i.e., that it has a memory, such that a second IC rapidly following the first can transit faster than if the transport events
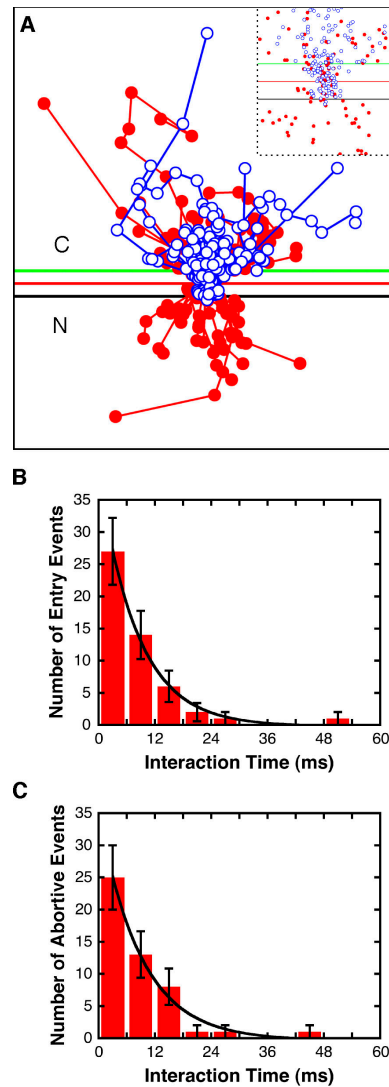

Figure 2. **Single-molecule trajectories and interaction times for cargos that entered the nucleus and for cargos that aborted transport.** (A) Alignment (see Materials and methods) of 43 trajectories from 19 NPCs (2 nuclei) under the conditions of Fig. 1. The red line is the experimentally determined position of the NE from the bright-field image; the green and black lines are for reference at −100 and +100 nm from the NE, respectively. Entry events are shown in red, and abortive events are shown in blue. N, nucleus; C, cytoplasm. (inset) Expanded view of the main figure (without lines connecting points for clarity), illustrating that cargos that underwent abortive transport appear to have had access to the same volume within the NE ± 100-nm region as the cargos that actually did transport. (B) Histogram of interaction times for cargos that entered the nucleus. τ = 8.0 ± 0.4 ms; n = 51. (C) Histogram of interaction times for cargos that underwent abortive transport. τ = 8.6 ± 0.7 ms; n = 49. For comparison, the interaction time for all observed cargos, including those for which both entry and exit compartment could not be determined, was 8.6 ± 0.4 ms (n = 264). From the n values for the interaction time calculations in B and C, the import efficiency was calculated to be 51 ± 5%.

are more infrequent. However, because Imp β–Imp α and Imp β–RanGTP complexes, as well as Imp β alone, bind to NPCs (Görlich et al., 1995, 1996; Moroianu et al., 1995; Kose et al., 1997; Kutay et al., 1997), we tested whether the Imp β concentration alone could modulate the interaction time and the import efficiency. The cargo concentration was fixed at 0.1 nM, and the Imp β concentration was increased from 0.1 to 15 μM.
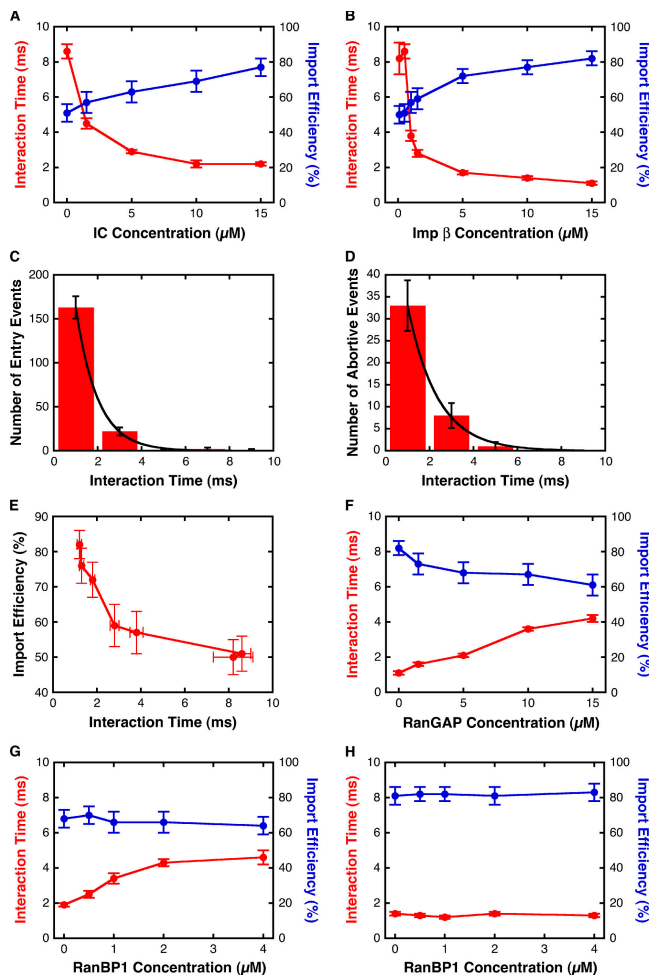
Figure 3. **NLS–2xGFP interaction time and import efficiency dependence on the bulk IC, cargo-free Imp β, RanGAP, and RanBP1 concentrations.** Unless otherwise noted, concentrations and the fluorescent cargo are the same as in Fig. 1. (A) Interaction time (red) and import efficiency (blue) dependence on IC concentration. The fluorescent cargo concentration was fixed at 0.1 nM, and the total cargo concentration was increased by adding "nonfluorescent" cargo (NLS-2xGFP[4C] with no fluorescent dye labels). At the cargo and cofactor concentrations used, >99% of the cargo was assumed to be complexed with Imp α and β (Catimel et al., 2001). Thus, the IC concentration was assumed to equal the added cargo concentration. When [IC] was ∼0.1 nM, [nonfluorescent cargo] = 0 nM and [Imp α] = [Imp β] = 0.5 μM. For all other IC concentrations, [Imp α] = [Imp β] = [nonfluorescent cargo]. (B) Interaction time (red) and import efficiency (blue) dependence on Imp β concentration. (C) Histogram of interaction times for cargos in B at 15 μM Imp β that entered the nucleus. τ = 1.0 ± 0.1 ms; n = 189. (D) Histogram of interaction times for cargos in B at 15 μM Imp β that underwent abortive transport. τ = 1.4 ± 0.1 ms; n = 42. (E) Nonlinear dependence of import efficiency on interaction time under certain conditions. The data in B were plotted to explicitly demonstrate the nonlinear relationship between import efficiency and interaction time when these values were varied by changing the Imp β concentration. (F) Interaction time (red) and import efficiency (blue) dependence on RanGAP concentration. [Imp β] = 15 μM. (G) Interaction time (red) and import efficiency (blue) dependence on RanBP1 concentration at low Imp β concentration. [Imp β] = 3 μM. [RanGAP] = 0.5 μM. (H) Interaction time (red) and import efficiency (blue) dependence on RanBP1 concentration at high Imp β concentration. [Imp β] = 15 μM. [RanGAP] = 0.5 μM.

The results (Fig. 3 B) were similar to those obtained by increasing the cargo and cofactor concentrations simultaneously, though the changes were slightly larger. These data are consistent with the hypothesis that similar initial IC and cargo-free

Imp β concentrations rapidly lead to similar numbers of Imp β molecules/complexes within the NPC and that these Imp β molecules/complexes within the NPC influence interaction times and import efficiencies. The sharp decrease in interaction time observed as the Imp β concentration was increased from 0.5 to 1.5 μM (Fig. 3 B, red) is consistent with a picture in which the binding of many Imp β molecules/complexes (K_d ∼1 μM, approximated from the transition point in this figure; similar to the K_d of ≥4 μM estimated for transportin [Ribbeck and Görlich, 2001]) to the NPC results in a decrease in cargo interaction time. The significant decrease in interaction times and increase in import efficiencies observed at high Imp β concentrations were not a consequence of an increased Imp β/Ran ratio because the interaction times and import efficiencies at 1.5 μM Imp β with 2 or 6 μM Ran (and 1 or 3 μM NTF2, respectively) were similar (Table S1, available at http://www.jcb.org/cgi/content/full/jcb.200605053/DC1). At 15 μM Imp β, the NPC interaction times for entry and abortive events were 1.0 ± 0.1 and 1.4 ± 0.1 ms, respectively (Fig. 3, C and D; see the supplemental text for an explanation of differences between the interaction times of entry and abortive events). Interaction time and import efficiency were not linearly related (Fig. 3 E), indicating that different sets of parameters determine these two transport characteristics.

Effect of GTP hydrolysis rate on interaction time and transport efficiency

We next tested the effect of RanGAP and RanBP1 on interaction time and import efficiency. RanGAP activates the Ran GTPase, causing rapid GTP hydrolysis (Bischoff et al., 1994). RanBP1 binds Imp β–RanGTP complexes and recruits RanGAP (Bischoff et al., 1995). We first determined the interaction time and import efficiency in the presence of increasing concentrations of RanGAP (0–15 μM) at a high initial cargo-free Imp β concentration (15 μM). A significant increase in the interaction time and decrease in the import efficiency was observed (Fig. 3 F). These data are consistent with the hypothesis that RanGAP promotes the conversion of RanGTP to RanGDP and that the reduced RanGTP concentration in the pore results in an increased interaction time and decreased import efficiency.

Because RanBP1 enhances the RanGAP-induced GTP hydrolysis rate of RanGTP by ∼10-fold (Bischoff et al., 1995), we tested the effect of RanBP1 on the interaction time and import efficiency. At 0.5 μM RanGAP and 3 μM Imp β, the interaction time increased, and the import efficiency stayed constant as the RanBP1 concentration was increased from 0 to 15 μM (Fig. 3 G). These results support the hypothesis that RanBP1 enhances RanGAP activity at the NPC and that a reduced RanGTP concentration within the NPC leads to an increased interaction time. The fact that the import efficiency stayed constant (within our errors) provides additional support for the conclusion drawn from Fig. 3 E that interaction time and import efficiency are distinct transport characteristics determined by different sets of parameters. In contrast, at 0.5 μM RanGAP and 15 μM Imp β, no effect of 0–15 μM exogenous RanBP1 was observed (Fig. 3 H). These results are consistent with the hypothesis that the RanBP1 enhancement of RanGAP activity at
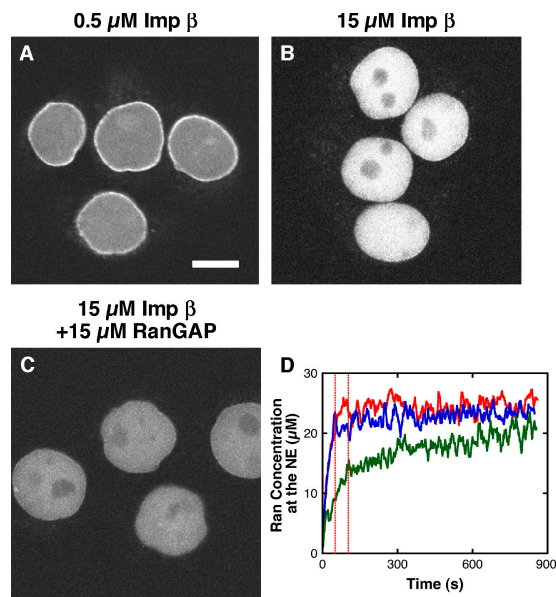
Figure 4. **Ran accumulation in the nucleus and at the NE.** (A–C) Nuclear accumulation of fluorescent Ran. Shown is the average of 101 confocal frames collected between 600 and 800 s after reaction initiation. Images were acquired under the same conditions and displayed with the same scaling. Unless noted above the images, concentrations were the same as in Fig. 1. Bar, 10 μm. (D) Time course of the NE accumulation of Ran under the conditions of A (red), B (blue), and C (green). The vertical dashed lines (red) indicate the time interval during which single-molecule transport experiments were conducted (unless otherwise noted).

the NPC is kinetically slower than the influx of RanGTP under these higher Imp β conditions.

To confirm the picture that activation of the Ran GTPase increased the rate at which RanGTP was converted to RanGDP and that the RanGTP concentration at the NPC affected the interaction time and import efficiency, we examined the effect of a nonhydrolyzable GTP analogue, guanosine 5′-(β-γ-imido)-triphosphate (GMP-PNP), on these transport characteristics. We first examined the role of GTP hydrolysis in NLS-2xGFP import at 0.5 μM Imp β. We observed an interaction time of 3.7 ± 0.2 ms and import efficiency of $63 \pm 5\%$ in the presence of 1 mM GMP-PNP. These data indicate that the NLS-2xGFP cargo was efficiently transported through NPCs in the presence of non-hydrolyzable GTP, as is expected for a 57-kD signal-dependent cargo (Lyman et al., 2002). We next examined the effect of RanGAP at 15 μM Imp β and 1 mM GMP-PNP. We observed an interaction time of 1.3 ± 0.1 and 1.2 ± 0.1 ms and import efficiencies of 78 ± 5 and $80 \pm 5\%$ at 0 and 15 μM RanGAP, respectively. Thus, unlike when hydrolysable GTP was present (Fig. 3 F), RanGAP had no effect in these experiments. These data therefore confirm that RanGAP increased the interaction time and decreased the import efficiency through its ability to promote GTP hydrolysis. The shorter interaction time and higher import efficiency observed with 1 mM GMP-PNP and 0.5 μM Imp β (3.7 ± 0.2 ms; $63 \pm 5\%$) compared with that observed with 1 mM GTP and 0.5 μM Imp β (8.6 ± 0.4 ms; $51 \pm 5\%$; see Fig. 3 B) is consistent with the picture that the GMP-PNP effects arise from a high RanGTP (RanGMP-PNP) concentration in the NPC as a result of the inability to form RanGDP.

## Role of Imp β in regulating interaction time and transport efficiency

To estimate the extent to which transport cofactors bound to NPCs under the conditions of the single-molecule transport measurements, confocal microscopy was used to examine the localization of fluorescent versions of Ran, Imp α, and Imp β. At both low and high Imp β concentrations, the Ran concentration at the NE increased to a steady-state value within ∼1 min after reaction initiation (Fig. 4). In contrast, the Imp β concentration at the NE continuously increased over a 15-min time frame. Imp α accumulated at the NE to a lesser extent than Imp β under these conditions, indicating that at least some Imp β accumulated in the absence of Imp α (Fig. 5). Despite the variation in Imp β concentration at the NE during the acquisition of single-molecule transport data, a higher mean Imp β concentration at the NE was present at higher bulk Imp β concentrations (Fig. 5 G). In addition, RanGAP reduced both the Imp β and Ran concentrations at the NE (Fig. 4 D and Fig. 5 G), indicating that an increased Ran GTPase activity led to a decrease in both the Ran and Imp β concentrations at the NE. The Ran concentration at the NE varied within a narrower range and, in some cases, was lower than the Imp β concentration at the NE (Figs. 4 D and 5 G), suggesting that some of the Imp β that accumulated in the NPCs in our single-molecule experiments was not complexed with Ran (consistent with the findings of Görlich et al. [1996]). Comparing these results with the single-molecule transport measurements, the general conclusion is that shorter interaction times and greater transport efficiencies were obtained when higher Imp β concentrations were observed at the NE.

As an additional test of the hypothesis that the accumulation of Imp β within the NPCs influenced the interaction time and transport efficiency, single-molecule transport measurements were made at 0.5 μM Imp β 15–16 min after reaction initiation, where the mean Imp β concentration at the NE was approximately fivefold higher than at 1–2 min after reaction initiation (Fig. 5 G). Under these conditions, the interaction time was 1.9 ± 0.1 ms and the import efficiency was $71 \pm 6\%$. These values are significantly different from the values obtained at 0.5 μM Imp β 1–2 min after reaction initiation (Fig. 3 B). These data support the hypothesis that a higher Imp β concentration in the NPC leads to a shorter interaction time and greater transport efficiency. However, a similarly high concentration of Imp β was observed at the NE at 0.5 μM Imp β after a 15–16-min time delay and at 15 μM Imp β plus 15 μM RanGAP with a 1–2-min time delay (Fig. 5 G), and yet the interaction time was significantly different under these conditions. This finding supports the hypothesis that the concentration of Imp β within NPCs is not the sole determinant of the interaction time in these experiments.

Signal-independent cargos

We next monitored the diffusion of a 10-kD dextran and the S13 protein of the small ribosomal subunit (rpS13; ∼18 kD) through NPCs under very low concentration conditions (0.1 nM) in the absence of transport cofactors, GTP, and glycerol. The NPC interaction times were 2.2 ± 0.1 and 3.3 ± 0.1 ms for

Figure 5. Imp α and β accumulation in the nucleus and at the NE. Unless noted at the top, concentrations were the same as in Fig. 1. Images shown in A–F are the average of 101 confocal frames collected between 600 and 800 s after reaction initiation. (A–C) Nuclear accumulation of fluorescent Imp β. Images were acquired under the same conditions and are displayed with the same scaling. (D–F) Nuclear accumulation of fluorescent Imp α. Images were acquired under the same conditions and are displayed with the same scaling (scaling different from A–C). Bars, 10 μm. (G) Time course of the NE accumulation of Imp β under the conditions of A (red), B (blue), and C (green). (H and I) Time course of the Imp β and α distribution under the conditions of A and D, respectively. The fluorescence intensity in the nuclear (blue), NE (red), and cytoplasmic (green) regions shows minimal NE accumulation of Imp α but significant NE accumulation of Imp β, compared with the cytoplasmic background. The estimated NE accumulation of Imp α could result primarily from the difficulty of distinguishing the nucleoplasm from the NE. The vertical dashed lines (red) in G–I indicate the time interval during which single-molecule transport experiments were conducted (unless otherwise noted).
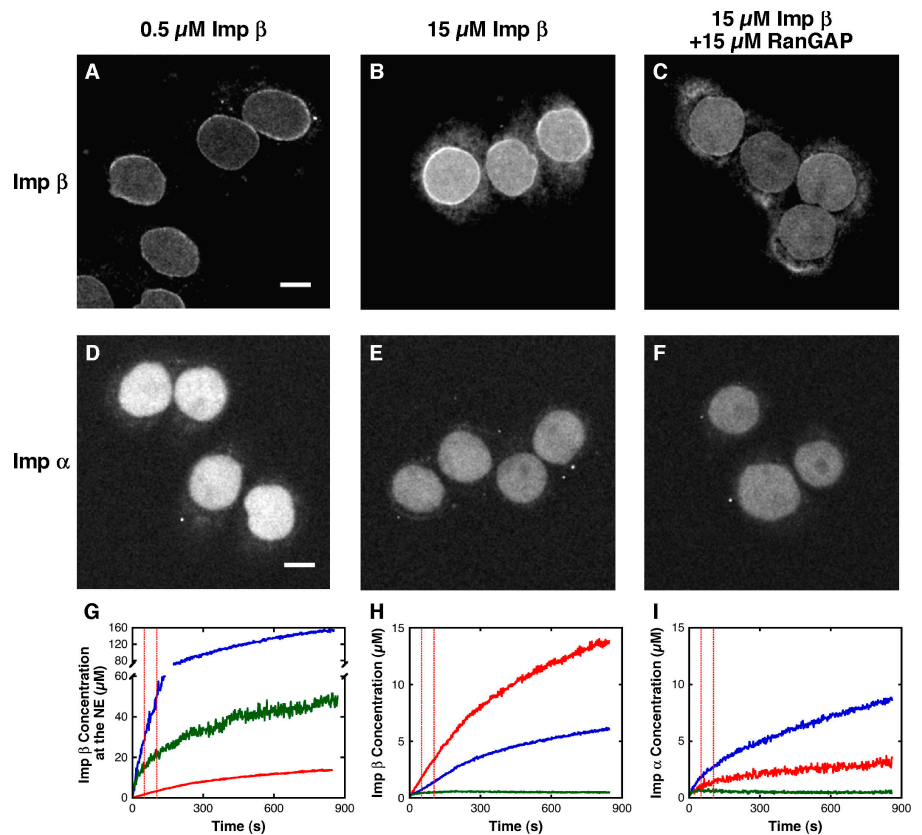
the dextran and rpS13, respectively. When 25% glycerol was added to the import buffer, the interaction times were 2.2 ± 0.2 and 3.2 ± 0.3 ms, respectively, indistinguishable from the previous measurements made in the absence of glycerol (Fig. 6). These data indicate that an approximately twofold increase in bulk solution viscosity did not affect the interaction time of the dextran and rpS13 cargos. Import efficiency values in the 25% glycerol import buffer for dextran and the rpS13 were 51 ± 6 and 50 ± 6%, respectively. The interaction frequencies of the dextran and rpS13 cargos were ~2.6- and ~1.8-fold higher, respectively, than that of the NLS-2xGFP cargo at the same concentration (Table S1). These data are consistent with the two- to threefold larger diffusion constant expected for the small cargos compared with that of the NLS-2xGFP ICs based on their molecular masses. Therefore, the measured interaction times for the signal-independent cargos do not arise from a few long, statistically unlikely events of a process occurring faster than our time resolution.

We then tested the effect of Imp β on dextran transport. As the Imp β concentration was increased from 0 to 3 μM Imp β, the interaction time decreased and the import efficiency increased (Fig. 7). At 15 μM Imp β, fluorescent dextran molecules were observed in the nucleus, demonstrating that the dextran molecules could still pass through the NPCs but that the interaction time was too fast to be measured (<0.5 ms). These data indicate that the interaction time for signal-independent cargos was strongly dependent on the concentration of Imp β. Because there was no Ran or GTP added in these experiments, the observed effects were due to Imp β alone.

In vivo nuclear import

As a control to the applicability of our results to in vivo nuclear import, cargos were microinjected into live HeLa cells at 37°C. Individual molecules were first observed diffusing in the cytoplasm.
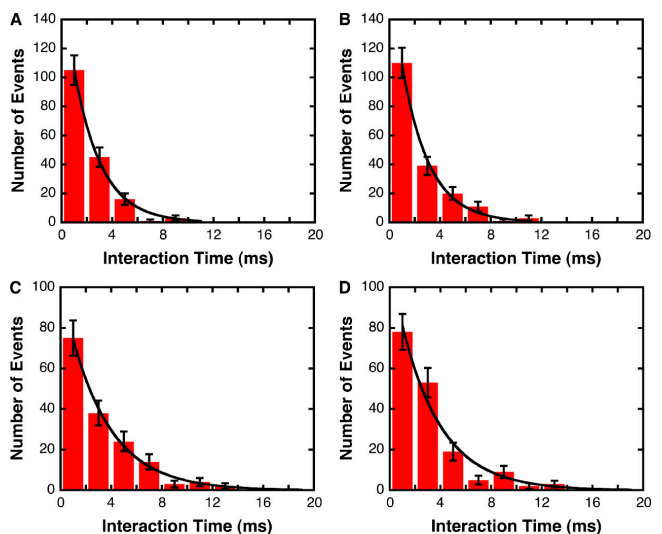

Figure 6. **Interaction times and transport efficiencies of signal-independent cargos.** Interaction times were determined in the absence of all exogeneous transport cofactors and GTP. (A) Histogram of 10-kD dextran interaction times in import buffer (no glycerol). τ = 2.2 ± 0.1; n = 170. (B) Histogram of 10-kD dextran interaction times in import buffer with 25% glycerol. τ = 2.2 ± 0.2; n = 184. (C) Histogram of rpS13 interaction times in import buffer (no glycerol). τ = 3.3 ± 0.1; n = 161. (D) Histogram of rpS13 interaction times in import buffer with 25% glycerol. τ = 3.2 ± 0.3; n = 171.
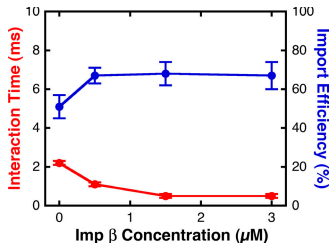
Figure 7. **10-kD dextran interaction time and import efficiency dependence on the Imp β concentration.** Interaction time (red) and import efficiency (blue) of 10-kD dextran in import buffer with 25% glycerol.

With time, cargos were observed interacting with the NE and transporting into the nucleus. The interaction time and import efficiency of NLS-2xGFP were 8.1 ± 0.1 ms and 51 ± 6%, respectively. The interaction time and import efficiency of the 10-kD dextran were 1.8 ± 0.1 ms and 50 ± 4%, respectively (Fig. 8). In *Xenopus laevis* eggs, the in vivo Imp β concentration is ∼3 μM (Ribbeck et al., 1998). In vitro measurements at 3 μM Imp β yielded significantly shorter interaction times and higher import efficiencies for NLS-2xGFP and the dextran than the in vivo values (Fig. 3, B and G; and Fig. 6 C). Possible (and nonexclusive) explanations that the in vivo data resemble in vitro data obtained at low Imp β concentrations include the following: (1) the in vivo Imp β concentration in HeLa cells is <3 μM, or a significant portion of Imp β is sequestered in our live cell experiments; (2) a low concentration of transport cofactors exists within NPCs with a full complement of transport cofactors and cargos (in vivo conditions), thereby resulting in an increased interaction time and decreased import efficiency; and (3) competition between additional import pathways and/or export pathways (in vivo conditions) results in a longer interaction time and lower import efficiency than expected for a relatively high concentration of transport cofactors within the NPC.

Discussion

Our SMF investigations of nuclear import have directly elucidated several fundamental properties of nucleocytoplasmic transport. The major findings reported here are as follows: (1) the import efficiency of both signal-independent and -dependent cargos is ∼50% in vivo and at low Imp β concentrations in vitro; (2) the interaction times of signal-independent cargos are not affected by an approximately two-fold increase in solvent viscosity; (3) for both signal-independent and -dependent cargos, the interaction time decreases and the import efficiency increases as the Imp β concentration increases; (4) for signal-dependent cargos, the interaction time can be modulated by changes in the GTP hydrolysis rate; and (5) though the interaction time and import efficiency are often negatively correlated, they are distinct characteristics determined by different sets of parameters. The implications of these findings are discussed below.

The primary message of the results reported here is that the interaction time and import efficiency vary with conditions. At sufficiently high cofactor and cargo concentrations, interac-
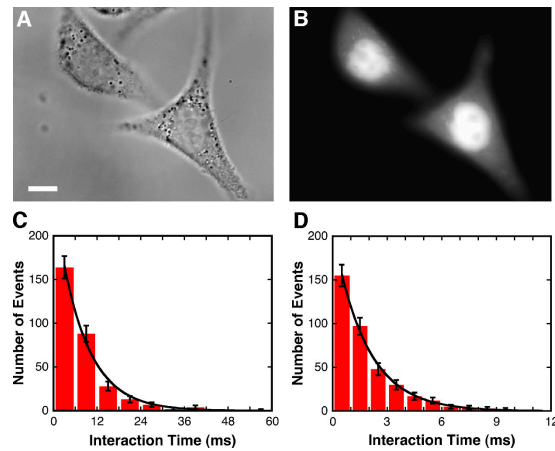

Figure 8. **In vivo single-molecule nuclear import.** (A) Bright-field image of two HeLa cells before microinjection. Bar, 10 μm. (B) Epifluorescence image of the two cells in A ∼3 min after cytoplasmic microinjection of NLS-2xGFP(4C). The Alexa 555–labeled cargo localized to the nuclei after microinjection. (C) Histogram of NE interaction times after microinjection of NLS-2xGFP(4C). Data were pooled from cargo tagged with Alexa 555 and cargo labeled with Alexa 647 (see Table S1, available at http://www.jcb.org/cgi/content/full/jcb.200605053/DC1). τ = 7.8 ± 0.4 ms (n = 307); import efficiency = 51 ± 5% (n = 115). (D) Histogram of NE interaction times after microinjection of Alexa 647 dextran (10 kD). τ = 1.8 ± 0.1 ms (n = 374); import efficiency = 50 ± 4% (n = 141).

tion time and import efficiency must limit the maximum rate of cargo transport (V_{max}). Assuming a linear relationship between V_{max} and the mean time to cross the NPC as predicted by the interaction time and import efficiency, the aforementioned data indicate that maximum signal-dependent cargo import rates can be modulated at least ∼10-fold by the Imp β concentration. Thus, V_{max} is variable. This conclusion could explain why the import rate does not follow simple Michaelis-Menten saturation kinetics for Imp β ICs and transportin but, rather, that "cooperativity" is observed at high transport cofactor concentrations (Ribbeck and Görlich, 2001; Yang et al., 2004). It may be generally true that as the Imp β–type transport cofactor concentration increases, the V_{max} increases. For all our NLS-2xGFP transport data, we observed a similar NPC interaction frequency, which suggests that an increased transport efficiency implies an increased bulk import rate. Under conditions where the transport rate is significantly less than the V_{max}, the interaction time is not expected to limit import rate. Thus, the magnitude by which changes in interaction time affect bulk transport rates remains uncertain.

The most parsimonious explanation for the observed changes in interaction time and import efficiency is that an NPC's transport properties can vary significantly depending on the particular molecules bound to it at any given moment in time. Thus, we introduce "pore occupancy," a term that recognizes that the number, identity, and distribution of molecules within the FG network affects cargo translocation through the NPC. The term pore occupancy is thus multivariate, explicitly including the concentration and distribution of all molecules within the pore, such as RanGTP, RanGDP, importins, exportins, and cargos. We have shown here that higher Imp β concentrations lead to altered pore occupancy conditions. The altered

pore occupancy conditions produced by high Imp β concentrations resulted, in general, in faster cargo translocation and higher transport efficiency. We have determined that higher numbers of Imp β molecules exist at the NE at high bulk Imp β concentrations. Though it is uncertain whether the distribution or concentration of RanGTP in the NPC changed as the bulk Imp β concentration changed, the total Ran concentration at the NE remained essentially unchanged (Fig. 4 D). Thus, the distribution of transport cofactors within the NPC under various pore occupancy conditions remains unclear and is likely different for different conditions.

Our findings with regard to signal-independent cargos challenge the assumption present in most published models (implicitly or explicitly) that small cargos diffuse through an open central channel. From nuclear accumulation measurements on dextrans, the putative central aqueous channel permitting passage of small cargos has been estimated to have a diameter of ~10.8 nm and a length of ~45 nm (Keminer and Peters, 1999). The viscosity of our import buffer with 25% glycerol is ~3.5 cP, and we consider this a reasonable conservative estimate for the viscosity within the putative central channel in this buffer (see the supplemental text). Based on these channel dimensions, assuming a viscosity of 3.5 cP, and correcting for drag arising from the channel walls (Paine and Scherr, 1975), a 10–18-kD cargo is predicted to one-dimensionally diffuse a distance corresponding to the length of this channel significantly faster (i.e., in ~40–70 μs) than our time resolution (1 ms). Based on this reasoning, the residence time of small cargos within the NPC's putative central channel should be unmeasurable with a 1-ms time resolution. Thus, the measured interaction times for signal-independent cargos at low Imp β concentrations were significantly longer than those expected for diffusional transport through the putative open central channel. Consistent with this observation, Ribbeck and Görlich (2001) found that, based on size alone, the transport flux of GFP (diameter ~5 nm) through NPCs is >10-fold slower than expected if transport occurs through the putative central channel. In addition, according to the central channel hypothesis, the interaction times of signal-independent cargos should increase with an increase in the viscosity within the channel. However, we observed that these interaction times were unchanged when the bulk viscosity was changed approximately twofold. Though these data appear inconsistent with the central channel model, we cannot rule out that edge effects within an open channel determine the transport characteristics of small cargos. In such a situation, the faster translocation of 10-kD dextran when the Imp β concentration within the FG network is high could be explained by structural changes or by a reduction in the strength of edge interactions (e.g., by Imp β coating the walls of the central channel).

Other investigators have reported Nup-deletion mutants where either the signal-independent or -dependent pathway, but not both, is affected, thus suggesting that the two pathways are distinct and unlinked (Shulga et al., 2000; Strawn et al., 2004) and supporting the central channel hypothesis. In contrast, the Imp β effects on signal-independent cargo transport suggest that these pathways partially overlap. Collectively, these data support the hypothesis that the two transport pathways are not identical, but they do share some elements. For example, signal-independent cargos could migrate through the same FG-Nup network through which signal-dependent cargos migrate. A relatively open, mesh-like, FG-Nup network could allow passage of small cargos while simultaneously prohibiting passage of larger cargos and allowing the passage of ICs (Ribbeck and Görlich, 2001). A convoluted migration path through such a meshwork is expected to be an inherently slower process than migration through an open channel, consistent with our data. An increase in bulk viscosity could have little effect on the microviscosity within the FG network because of an already relatively high viscosity introduced by molecular crowding and the ordering of solvent molecules in the porous network (Luby-Phelps, 2000; Liu et al., 2004).

The exact mechanism whereby the Imp β concentration influences interaction time is likely to be complex. As described more fully in the supplemental text, we consider that Imp β could play a direct and/or indirect role in influencing pore occupancy. As an example of a direct effect, the presence of a large number of Imp β molecules within the NPC could reduce the volume accessible to transiting cargos. A decreased available volume implies a lower entropy and, thus, an increased free energy for transiting molecules in the pore, which in turn suggests easier access to the rate-limiting transition state and, hence, faster escape (Minton, 2001). This mechanism is consistent with the shorter interaction times of the 10-kD dextran at high Imp β concentrations. As an example of an indirect effect, the presence of Imp β in the bulk solution or within the pore itself could change the distribution of RanGTP within the NPC. Riddick and Macara (2005) observed that under excess Imp β concentrations (e.g., [Imp β] > 2 μM), RanGTP is shuttled to the cytoplasmic compartment by cargo-free Imp β. Thus, both the distribution and concentration of RanGTP in the NPC or at the faces of the NPC could be significantly affected by the bulk Imp β concentration (without the total Ran concentration at the NE changing significantly; Fig. 4 C). A second possible indirect effect of higher Imp β concentrations is that Imp β molecules within the NPC could disrupt energetically favorable filament interactions (Ribbeck and Görlich, 2001). Consequently, high Imp β concentrations could increase the fluidity of the FG network (and, hence, the diffusion constant of the cargo within the pore). Thus, the faster translocation of signal-independent cargos in the presence of high Imp β concentrations could be explained, at least in part, by Imp β–induced structural changes in the FG network These Imp β–induced structural perturbations could also change the RanGTP distribution within the FG network or promote an increased productive interaction rate between ICs and RanGTP. The simple presence of many macromolecules of any type within the FG network may be sufficient to alter the physical properties of this network.

In conclusion, we emphasize that the pore occupancy model does not postulate a transport mechanism but, rather, suggests a general means by which cargo interaction times and transport efficiencies can be modulated. Therefore, the pore occupancy model is in principle entirely consistent with existing mechanistic models. Our data challenge the assumption of an

open central channel for small cargos, but the basic size-dependent exclusionary principles behind other mechanistic models are applicable with either an open central channel or a porous network allowing passage of small cargos, as we suggest here. The fact that the Imp β concentration influences interaction time and import efficiency for both signal-independent and -dependent cargos implies that a complete mechanistic model of NPC transport must consider the influence of other molecules within the NPC on cargo migration through the pore. The concentration range in which Imp β causes the greatest changes in interaction time is close to the estimated physiological Imp β concentration (∼3 μM; Ribbeck et al., 1998), suggesting that in vivo mechanisms in which Imp β is alternately sequestered and released, or in which expression levels are modulated (Hanz et al., 2003), could have dramatic effects on nuclear transport rates. Whether cells actively alter cargo interaction times and import efficiencies to regulate transport fluxes in response to cellular needs remains an open question.

Materials and methods

Proteins and transport conditions
Unless updated here, we followed our previously published methods (Yang et al., 2004; Yang and Musser, 2006). NLS-2xGFP(2C) has two exposed cysteines reactive with maleimides (Yang et al., 2004). To obtain a brighter cargo, two additional cysteine residues were added to NLS-2xGFP(2C) by mutating the surface serines on the bottom of the two GFP β-barrel domains (S175C) to yield NLS-2xGFP(4C) (Yang and Musser, 2006). The NLS-2xGFP(4C) mutant tagged with four Alexa 647 maleimide (Invitrogen) molecules is ∼1.8-fold more fluorescent than doubly labeled NLS-2xGFP(2C). Ribosomal protein S13 (rpS13) of the small ribosomal subunit was cloned (IMAGE clone 2899987; American Type Culture Collection) into pET9a (Novagen) with a HHHHHHC C-terminal tag, expressed in *Escherichia coli* BL21(λDE3) by 1 mM IPTG induction and purified by nickel-nitrilotriacetic acid Superflow (QIAGEN) and MonoS (GE Healthcare) chromatography. After labeling rpS13 with Alexa 555 maleimide (Invitrogen) and electrophoresing the protein on a polyacrylamide gel, a single fluorescent band was observed. All coding regions were confirmed by DNA sequencing. RanGAP and RanBP1 were expressed with N-terminal 6xHis-tags (plasmids were a gift from D. Görlich, University of Heidelberg, Heidelberg, Germany) and purified as described previously (Kutay et al., 1997). Fluorescent versions of Imp α, Imp β, and Ran were obtained by 10–60-min reaction with Alexa 555 maleimide, yielding a mean labeling of ∼3.3, ∼0.5, and ∼2 dye molecules per protein molecule, respectively. The fluorescent transport cofactors were functional in nuclear transport assays. The 10-kD dextran was obtained from the manufacturer (Invitrogen) labeled with a mean of 1–1.5 Alexa 647 molecules. The buffer used for import experiments was 20 mM Hepes, pH 7.3, 1.5% polyvinylpyrrolidone (360 kD), 110 mM KOAc, 5 mM NaOAc, 2 mM MgOAc, and 1 mM EGTA (import buffer). Glycerol was added where indicated.

Instrumentation
The SMF microscope setup included a microscope (Axiovert 200M; Carl Zeiss MicroImaging, Inc.) equipped with a 1.45 NA 100× oil-immersion objective (Carl Zeiss MicroImaging, Inc.), an on-chip multiplication gain charge-coupled device camera (Cascade 128; Roper Scientific), and the MetaMorph software package (Universal Imaging Corp.) for data acquisition and processing. An I-Pentamax (Roper Scientific) was used for some in vivo experiments. High spatial resolution bulk transport images were obtained with a camera (CoolSnapES; Roper Scientific). A microinjector (FemtoJet; Eppendorf) and objective warmer (Bioptechs) was used for live cell injection at 37°C. Sample temperature was maintained by thermal contact with the immersion oil. Using 1.0-μm TetraSpeck microspheres (Invitrogen), we determined that the bright-field and SMF images were aligned to within 13 ± 2 nm (*n* = 10). In single-molecule experiments, a 300-mW, 532-nm solid-state laser (Coherent Radiation) was used for Alexa 555 excitation (9 kW/cm² measured at the specimen). A 2.5-W ArKr mixed-gas ion laser (Spectra-Physics) was used for Alexa 647 excitation

(647 nm; 4 kW/cm²). Control experiments revealed indistinguishable interaction times for cargo labeled with Alexa 555 or 647 (Fig. S1 and the supplemental text). The Alexa 647 dye was necessary for high "nonfluorescent" cargo concentrations because of the leakage of GFP fluorescence onto the Alexa 555 fluorescence channel.

An inverted confocal microscope (TCS SP2 AOBS; Leica) was used to determine nuclear and NE accumulation of transport cofactors and cargos. Transport cofactor concentrations in the nucleus and at the NE were estimated by comparison with the fluorescence far from the cells.

Calculation of the import efficiency
Accurate import efficiency estimates are obtained only when the analysis includes single-molecule trajectories in which a cargo complex has interacted with an NPC. For molecules that crossed the NE, an NPC interaction was assumed because NPCs are the only known route of passage across the NE. The major challenge was to reliably infer when a molecule interacted with an NPC but did not transport across the NE. Our solution was as follows. Based on fluorescence recovery after photobleaching measurements (Daigle et al., 2001; Rabut et al., 2004) and our earlier results (Yang et al., 2004), we assumed that the NPCs remained within a small circular area (*r* < 100 nm) for the duration of our experiments. An overlay of all trajectories in which molecules clearly passed through an NPC identified the location of all functional NPCs within the imaging area (Yang et al., 2004). At least three such NE crossing events were observed for every NPC included in our analysis. We defined three classes of trajectories for cargos that approached within 100 nm of the NE from the cytoplasmic side. The first class (Fig. 2 A, red) consists of trajectories for which the first and last points are at least 100 nm from the NE, and a line between these points crosses the NE (entry and exit compartments different). This class is considered to consist of those molecules that transported across the NE (entry events). The second class (Fig. 2 A, blue) consists of trajectories for which (1) the first and last points are at least 100 nm away from the NE and both are on the cytoplasmic side of the NE and (2) at least one point is within 100 nm of an NPC location. Because the span from the tips of the cytoplasmic filaments to the center of the NPC is ∼100 nm (the NE, i.e., the red line in Fig. 2 A, was assumed to pass through the center of the NPC), this class of trajectories identifies those cargo complexes that potentially interacted with an NPC for at least one frame but did not transport. Therefore, this second class is considered to consist of molecules that interacted with an NPC but did not transport through the NPC (abortive events). The third class consists of trajectories that did not fall into either the first or second class (i.e., the exit compartment was unclear) and were discarded from further consideration in import efficiency calculations. Thus, import efficiency is the number of class 1 trajectories divided by the number of class 1 and 2 trajectories and is reported as a percentage.

Trajectory alignment
The trajectory alignment in Fig. 2 A was performed as follows. For entry events, all trajectories were aligned based on their NE crossing point. If there were multiple NE crossing points in a given trajectory, the mean crossing point was used. For abortive events, the horizontal-centroid of the points within the NE ± 100-nm region was placed on the vertical axis defined by the NE crossing points of the entry events. All trajectories were rotated so that the plane of the NE in the alignment corresponds to the plane of the NE at the NPC from which the trajectories were obtained. This procedure centered the trajectories about a single NPC position.

Microinjection
Freshly split HeLa cells were grown overnight at 37°C with 5% CO₂ in DME (Invitrogen) supplemented with 4.5 g/l glucose, 862 mg/l GlutaMAX-I, 15 mg/ml phenol red, 100 U/ml penicillin, 100 μg/ml streptomysin, and 10% (vol/vol) newborn calf serum in glass-bottomed Petri dishes (MatTek). Immediately before microinjections, the media was replaced with identically supplemented DME without phenol red. Cargo was diluted to ∼0.1 nM (single-molecule transport) or 0.5 μM (bulk transport) with 10 mM Tris, pH 7.3, 100 mM NaCl, and 0.1% polyvinylpyrrolidone (40 kD) and injected in a single 0.8-s pulse.

Data analysis
All errors are 68% confidence intervals, unless otherwise indicated.

Online supplemental material
Fig. S1 shows control experiments that suggest that NLS-2xGFP transport was not affected by 25% glycerol or dyes on the protein. Fig. S2 shows that nuclear accumulation of cargo was optimal at ∼2 μM Ran at both

low and high Imp β concentrations. Fig. S3 demonstrates how viscosity was estimated from single-molecule diffusion measurements. Fig. S4 compares NE localization by bright-field and fluorescence imaging methods. Table S1 summarizes the interaction times, import efficiencies, and interaction frequencies for the various conditions discussed in this paper. Video 1 shows the entry event in Fig. 1. Video 2 shows the abortive event in Fig. 1. Online supplemental material is available at http://www.jcb.org/cgi/content/full/jcb.200605053/DC1.

References

Bayliss, R., K. Ribbeck, D. Akin, H.M. Kent, C.M. Feldherr, D. Görlich, and M. Stewart. 1999. Interaction between NTF2 and xFxFG-containing nucleoporins is required to mediate nuclear import of RanGDP. *J. Mol. Biol.* 293:579–593.

Ben-Efraim, I., and L. Gerace. 2001. Gradient of increasing affinity of importin β for nucleoporins along the pathway of nuclear import. *J. Cell Biol.* 152:411–417.

Bischoff, F.R., and D. Görlich. 1997. RanBP1 is crucial for the release of RanGTP from importin β-related nuclear transport factors. *FEBS Lett.* 419:249–254.

Bischoff, F.R., C. Klebe, J. Kretschmer, A. Wittinghofer, and H. Ponstingl. 1994. RanGAP1 induces GTPase activity of nuclear Ras-related Ran. *Proc. Natl. Acad. Sci. USA.* 91:2587–2591.

Bischoff, F.R., H. Krebber, E. Smirnova, W. Dong, and H. Ponsting. 1995. Co-activation of RanGTPase and inhibition of GTP dissociation by Ran-GTP binding protein RanBP1. *EMBO J.* 14:705–715.

Catimel, B., T. Teh, M.R.M. Fontes, I.G. Jennings, D.A. Jans, G.J. Howlett, E.C. Nice, and B. Kobe. 2001. Biophysical characterization of interactions involving importin α during nuclear import. *J. Biol. Chem.* 276:34189–34198.

Coutavas, E., M. Ren, J.D. Oppenheim, P. D'Eustachio, and M.G. Rush. 1993. Characterization of proteins that interact with the cell-cycle regulatory protein Ran/TC4. *Nature.* 366:585–587.

Cronshaw, J.M., A.N. Krutchinsky, W. Zhang, B.T. Chait, and M.J. Matunis. 2002. Proteomic analysis of the mammalian nuclear pore complex. *J. Cell Biol.* 158:915–927.

Daigle, N., J. Beaudouin, L. Hartnell, G. Hallberg, J. Lippincott-Schwartz, and J. Ellenberg. 2001. Nuclear pore complexes form immobile networks and have a very low turnover in live mammalian cells. *J. Cell Biol.* 154:71–84.

Denning, D.P., S.S. Patel, V. Uversky, A.L. Fink, and M. Rexach. 2003. Disorder in the nuclear pore complex: the FG repeat regions of nucleoporins are natively unfolded. *Proc. Natl. Acad. Sci. USA.* 100:2450–2455.

Dworetzky, S.I., and C.M. Feldherr. 1988. Translocation of RNA-coated gold particles through the nuclear pores of oocytes. *J. Cell Biol.* 106:575–584.

Fahrenkrog, B., and U. Aebi. 2003. The nuclear pore complex: nucleocytoplasmic transport and beyond. *Nat. Rev. Mol. Cell Biol.* 4:757–766.

Feldherr, C.M., E. Kallenbach, and N. Schultz. 1984. Movement of karyophilic protein through the nuclear pores of oocytes. *J. Cell Biol.* 99:2216–2222.

Fried, H., and U. Kutay. 2003. Nucleocytoplasmic transport: taking an inventory. *Cell. Mol. Life Sci.* 60:1659–1688.

Görlich, D., F. Vogel, A.D. Mills, E. Hartmann, and R.A. Laskey. 1995. Distinct functions for the two importin subunits in nuclear protein import. *Nature.* 377:246–248.

Görlich, D., N. Panté, U. Kutay, U. Aebi, and F.R. Bischoff. 1996. Identification of different roles for RanGDP and RanGTP in nuclear protein import. *EMBO J.* 15:5584–5594.

Görlich, D., M.J. Seewald, and K. Ribbeck. 2003. Characterization of Ran-driven cargo transport and the RanGTPase system by kinetic measurements and computer simulation. *EMBO J.* 22:1088–1100.

Hanz, S., E. Perlson, D. Willis, J.-Q. Zheng, R. Massarwa, J.J. Huerta, M. Koltzenburg, M. Kohler, J. van-Minnen, J.L. Twiss, and M. Fainsilber.

2003. Axonplasmic importins enable retrograde injury signaling in lesioned nerve. *Neuron.* 40:1095–1104.

Izaurralde, E., U. Kutay, C. von Kobbe, I.W. Mattaj, and D. Görlich. 1997. The asymmetric distribution of the constituents of the Ran system is essential for transport into and out of the nucleus. *EMBO J.* 16:6535–6547.

Keminer, O., and R. Peters. 1999. Permeability of single nuclear pores. *Biophys. J.* 77:217–228.

Koepp, D.M., and P.A. Silver. 1996. A GTPase controlling nuclear trafficking: running the right way or walking RANdomly? *Cell.* 87:1–4.

Kose, S., N. Imamoto, T. Tachibana, T. Shimamoto, and Y. Yoneda. 1997. Ran-unassisted nuclear migration of a 97-kD component of nuclear pore-targeting complex. *J. Cell Biol.* 139:841–849.

Kutay, U., E. Lizaurralde, F.R. Bischoff, I.M. Mattaj, and D. Görlich. 1997. Dominant-negative mutants of importin-beta block multiple pathways of import and export through the nuclear pore complex. *EMBO J.* 16:1153–1163.

Liu, Y., Q. Wang, and L. Lu. 2004. Transport properties and distribution of water molecules confined in hydrophobic nanopores and nanoslits. *Langmuir.* 20:6921–6926.

Luby-Phelps, K. 2000. Cytoarchitecture and physical properties of cytoplasm: volume, viscosity, diffusion, intracellular surface area. *Int. Rev. Cytol.* 192:189–221.

Lyman, S.K., T. Guan, J. Bednenko, H. Wodrich, and L. Gerace. 2002. Influence of cargo size on Ran and energy requirements for nuclear protein import. *J. Cell Biol.* 159:55–67.

Macara, I.G. 2001. Transport into and out of the nucleus. *Microbiol. Mol. Biol. Rev.* 65:570–594.

Minton, A.P. 2001. The influence of macromolecular crowding and macromolecular confinement on biochemical reactions in physiological media. *J. Biol. Chem.* 276:10577–10580.

Moroianu, J., M. Hijikata, G. Blobel, and A. Radu. 1995. Mammalian karyopherin $\alpha_1\beta$ and $\alpha_2\beta$ heterodimers: α_1 or α_2 subunit binds nuclear localization signal and β subunit interacts with peptide repeat-containing nucleoporins. *Proc. Natl. Acad. Sci. USA.* 92:6532–6536.

Nachury, M.V., and K. Weis. 1999. The direction of transport through the nuclear pore can be inverted. *Proc. Natl. Acad. Sci. USA.* 96:9622–9627.

Nakielny, S., and G. Dreyfuss. 1999. Transport of proteins and RNAs in and out of the nucleus. *Cell.* 99:677–690.

Paine, P.L., and P. Scherr. 1975. Drag coefficient for the movement of rigid spheres through liquid-filled cylindrical pores. *Biophys. J.* 15:1087–1091.

Panté, N., and M. Kann. 2002. Nuclear pore complex is able to transport macromolecules with diameters of about 39 nm. *Mol. Biol. Cell.* 13:425–434.

Peters, R. 2005. Translocation through the nuclear pore complex: selectivity and speed by reduction-of-dimensionality. *Traffic.* 6:421–427.

Pyhtila, B., and M. Rexach. 2003. A gradient of affinity for the karyopherin Kap95p along the yeast nuclear pore complex. *J. Biol. Chem.* 278:42699–42709.

Rabut, G., V. Doye, and J. Ellenberg. 2004. Mapping the dynamic organization of the nuclear pore complex inside single living cells. *Nat. Cell Biol.* 6:1114–1121.

Rexach, M., and G. Blobel. 1995. Protein import into nuclei: association and dissociation reactions involving transport substrate, transport factors, and nucleoporins. *Cell.* 83:683–692.

Ribbeck, K., and D. Görlich. 2001. Kinetics analysis of translocation through nuclear pore complexes. *EMBO J.* 20:1320–1330.

Ribbeck, K., G. Lipowsky, H.M. Kent, M. Stewart, and D. Görlich. 1998. NTF2 mediates nuclear import of Ran. *EMBO J.* 17:6587–6598.

Riddick, G., and I.G. Macara. 2005. A systems analysis of importin-α-β mediated nuclear protein import. *J. Cell Biol.* 168:1027–1038.

Rout, M.P. 2000. The yeast nuclear pore complex: composition, architecture, and transport mechanism. *J. Cell Biol.* 148:635–651.

Rout, M.P., and J.D. Aitchison. 2001. The nuclear pore complex as a transport machine. *J. Biol. Chem.* 276:16593–16596.

Rout, M.P., J.D. Aitchison, M.O. Magnasco, and B.T. Chait. 2003. Virtual gating and nuclear transport: the hole picture. *Trends Cell Biol.* 13:622–628.

Shulga, N., N. Mosammaparast, R. Wozniak, and D.S. Goldfarb. 2000. Yeast nucleoporins involved in passive nuclear envelope permeability. *J. Cell Biol.* 149:1027–1038.

Stoffler, D., B. Fahrenkrog, and U. Aebi. 1999. The nuclear pore complex: from molecular architecture to functional dynamics. *Curr. Opin. Cell Biol.* 11:391–401.

Stoffler, D., B. Feja, B. Fahrenkorg, J. Walz, D. Typke, and U. Aebi. 2003. Cryo-electron tomography provides novel insights into nuclear pore architecture: implications for nucleocytoplasmic transport. *J. Mol. Biol.* 328:119–130.

Strawn, L.A., T. Shen, N. Shulga, D.S. Golldfarb, and S.R. Wente. 2004. Minimal nuclear pore complexes define FG repeat domains essential for transport. *Nat. Cell Biol.* 6:197–206.

Walther, T.C., H.S. Pickersgill, V.C. Cordes, M.W. Goldberg, T.D. Allen, I.W. Mattaj, and M. Fornerod. 2002. The cytoplasmic filaments of the nuclear pore complex are dispensable for selective protein import. *J. Cell Biol.* 158:63–77.

Yang, W., and S.M. Musser. 2006. Visualizing single molecules interacting with nuclear pore complexes by narrow-field epifluorescence microscopy. *Methods.* 39:316–328.

Yang, W., J. Gelles, and S.M. Musser. 2004. Imaging of single-molecule translocation through nuclear pore complexes. *Proc. Natl. Acad. Sci. USA.* 101:12887–12892.

Yokoyama, N., N. Hayashi, T. Seki, N. Panté, T. Ohba, K. Nishii, K. Kuma, T. Hayashida, T. Miyata, U. Aebi, et al. 1995. A giant nucleopore protein that binds Ran/TC4. *Nature.* 376:184–188.